PCCP

Accepted Manuscript

ROYAL SOCIETY OF CHEMISTRY

www.rsc.org/pccp

Unassisted HI Photoelectrolysis Using n-WSe_2 Solar Absorbers

James R. McKone, Rebecca A. Potash, Francis J. DiSalvo, and Héctor D. Abruña*

Department of Chemistry and Chemical Biology
Cornell University
245 East Avenue Ithaca, NY 14850

*To whom correspondence should be addressed
E-mail: hda1@cornell.edu

Abstract. Molybdenum and tungsten diselenide are among the most robust and efficient semiconductor materials for photoelectrochemistry, but they have seen limited use for integrated solar energy storage systems. Herein, we report that n-type WSe_2 photoelectrodes can facilitate unassisted aqueous HI electrolysis to H_2(g) and HI_3(aq) when placed in contact with a platinum counter electrode and illuminated by simulated sunlight. Even in strongly acidic electrolyte, the photoelectrodes are robust and operate very near their maximum power point. We have rationalized this behavior by characterizing the n-WSe_2 | HI/HI_3 half cell, the Pt | HI/H_2 || HI_3/HI | Pt full cell, and the n-WSe_2 band-edge positions. Importantly, specific interactions between the n-WSe_2 surface and aqueous iodide significantly shift the semiconductor's flatband potential and allow for unassisted HI electrolysis. These findings exemplify the important role of interfacial chemical reactivity in influencing the energetics of semiconductor-liquid junctions and the resulting device performance.

Keywords: tungsten diselenide, photoelectrochemistry, solar storage, electrolysis, hydrogen, hydrioiodic acid, iodine, iodide, triiodide

Introduction

Semiconductor photoelectrochemistry has been extensively developed as a method for integrated solar energy capture and storage.[1–3] Promising results have been achieved recently, especially involving stabilization of efficient photovoltaic materials towards harsh aqueous acidic or alkaline environments.[4–12] However, the only full solar water electrolysis systems that have been demonstrated to operate as efficiently as photovoltaics have relied on semiconductor homojunctions, discrete solar cells, and/or complete isolation of the light absorber component from the water-splitting component.[13–20] These systems sacrifice the simplicity and elegance of the original device formulations for solar water splitting that used single metal oxide photoelectrodes coupled to purely catalytic auxiliary electrodes (Figure 1) but obtained very low energy conversion efficiencies.[1–3,21]

Electrolysis of hydrohalic acids (HX where X = I^-, Br^-, or Cl^-) represents an attractive alternative to water splitting for facilitating solar energy storage. Like water splitting, HX electrolysis results in hydrogen gas as an energy-dense product. Additionally, the kinetics of halide oxidation are markedly faster than water oxidation to O_2(g), and dihalogens can be used for value-added

processes such as water purification and chemical disinfection. Fuel cells based on HX species have also been shown to operate efficiently at high power densities.[22–24]

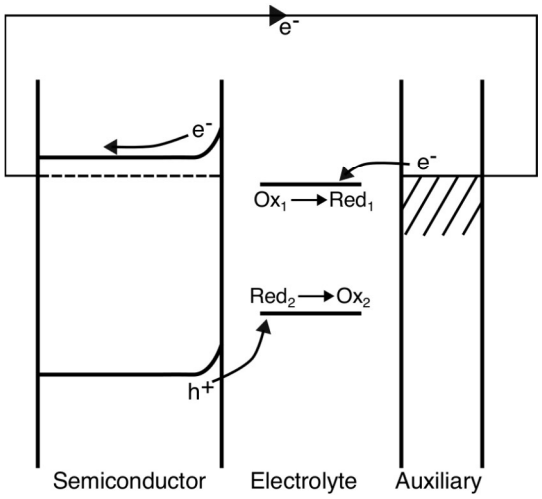

Figure 1. Band energy diagram illustrating the desirable energetic relationships for simultaneous oxidation and reduction of two sets of redox couples (Ox_1/Red_1 and Ox_2/Red_2, respectively) using a single photoelectrode short-circuited to a purely catalytic counter electrode, after Nozik and Memming.[3] The vertical axis represents electrochemical potential, while the horizontal axis represents distance normal to the semiconductor-electrolyte interface.

Several canonical semiconductor materials have been used previously for photoelectrochemical HX electrolysis.[25–28] Notably, the Texas Instruments company nearly commercialized a reversible solar energy storage system based on an HBr electrolyte using microspherical Si absorbers.[29] Therefore, electrolysis of HX species might be reasonably considered as an alternative or a stepping-stone to solar water splitting. Relatively little work has been carried out in this area during the last several decades, but promising results have been achieved recently for systems based on stabilized planar GaAs[30] and membrane-embedded Si microwire arrays.[31]

Layered metal chalcogenide (LMC) compounds such as $MoSe_2$ and WSe_2 are particularly attractive candidates for electrochemical solar energy storage involving halide oxidation. These materials have been demonstrated to drive photoelectrochemical iodide and bromide oxidation efficiently in aqueous electrolytes.[32–40] $MoSe_2$, in particular, has also exhibited remarkable stability under the harsh conditions of extended aqueous photoelectrochemical iodide oxidation.[41,42]

LMC compounds have also been used for net electrolysis of hydrohalic acids in systems employing redox mediators, multiple semiconductor absorbers, and unconventional electrochemical

configurations. Fan et al. reported iodide oxidation coupled with reduction of methyl viologen (MV^{2+}) via simultaneous illumination of an n-type WSe_2 photoanode and a p-type WSe_2 photocathode. The reduced MV^{+} could then be reversibly oxidized to yield H_2(g).[43] Levy-Clement et al. reported electrolysis of HBr and HI using n-WSe_2 photoanodes coupled to platinized p-InP photocathodes.[44] Notably, these researchers found that the photovoltage produced by WSe_2 combined with InP was more than sufficient to drive HI electrolysis, and electrical energy could also be extracted from the system. Bicelli and Razzini qualitatively observed the simultaneous generation of H_2(g) and I_2(s) from acidic iodide electrolytes on platinized n-WSe_2 crystals under high-intensity illumination in an optical microscope.[45] Baglio and coworkers also reported unassisted electrolysis of aqueous HI using n-type WS_2 photoelectrodes coupled to Pt auxiliary electrodes, although their experimental conditions prevented detailed characterization of the photoelectrode properties under operating conditions.[46]

Many of the previous reports of iodide oxidation at WSe_2 photoelectrodes indicate that photovoltages in excess of 600 mV can be obtained in such systems, implying that a single WSe_2 photoelectrode may be able to facilitate net electrolysis of HI alone. Surprisingly, though, no reports exist of unassisted HI splitting by n-WSe_2 using a simple two-electrode configuration (as in Figure 1). Herein we report just such a system, which yields current densities exceeding 10 mA cm^{-2} for n-WSe_2 photoelectrodes illuminated with polychromatic light approximating that of the solar spectrum. We have further characterized the individual behaviors of n-WSe_2 and Pt electrodes in contact with acidic iodide electrolytes, and we have carried out impedance spectroscopy to elucidate the energetics of the n-WSe_2 | HI interface. These experiments together allow for rationalization of the observed behavior of the n-WSe_2 | HI_3/HI || HI/H_2 | Pt cell. Interestingly, the ability of illuminated n-WSe_2 to split HI without electrical energy input stems directly from a shift in the band edge positions due to specific adsorption of iodide, which illustrates the importance of surface chemistry when evaluating the viability of semiconductors for energy conversion and storage reactions.

Experimental

N-type WSe_2 crystals were kindly provided by J. Wiensch, J. John, and N. S. Lewis of the California Institute of Technology. They were synthesized using a well-established chemical vapor transport procedure in sealed silica tubes using $TeCl_4$ as a transport agent and without extrinsic

doping sources.[41,47–49] The crystals were plate-like, up to ~1 cm^2 in area, and up to several hundred μm thick.

Crystals were cleaned of adventitious polycrystalline surface layers by sonicating briefly in 1 M KOH solution or by gently rubbing the crystal surfaces with cotton swabs. Then they were cut into pieces between 0.01 and 0.05 cm^2 in size and contacted on the rear by manual application of Ga/In eutectic. The crystals were connected to a bare copper wire using Ag paint (GC Electronics) and insulated using two-part epoxy (Hysol 1C or 9460). Annotated photographs of a complete electrode are shown in Figure 2. Geometric areas were measured using software analysis (ImageJ) of images collected from a calibrated flat-bed scanner (Epson Perfection V30) at 2400 pixels per inch.
In some cases, electrodes were etched according to a previously-reported method.[50] They were illuminated at ~1 Sun equivalent intensity and poised at 1.2 V versus Ag/AgCl in 0.1 M H_2SO_4(aq) for 5-30 minutes, resulting in formation of a translucent white surface layer of hydrous tungsten oxide. A brief rinse in 5 M KOH electrolyte removed the surface oxide to reveal a slightly roughened n-WSe_2 electrode that generally gave improved photocurrents compared to the un-etched crystal.

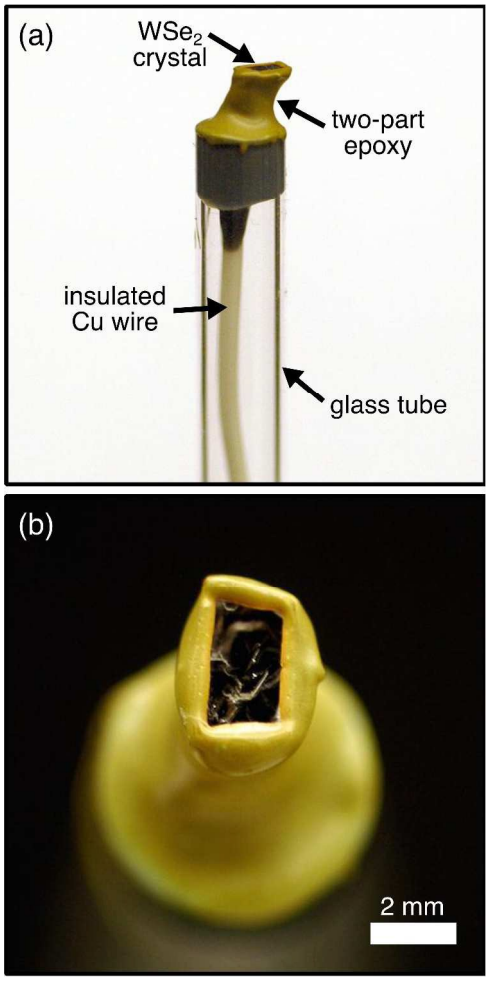

Figure 2. (a) Side view of an assembled n-type WSe_2 photoelectrode with the key components labeled. (b) Top view of the same photoelectrode showing the active surface area defined by a two-part epoxy. Features visible on the surface of the photoelectrode are step-edges that remain in spite of careful surface cleavage, and the red-brown coloration of the epoxy is due to staining from the iodide electrolyte.

Electrochemical and photoelectrochemical measurements were taken using either a single-compartment glass cell equipped with a flat optical glass window, or using a custom acrylic two-compartment cell. Additional details on the cell design are included in the Electronic Supporting Information (ESI). In all cases, solution agitation was provided using a PTFE-coated stir bar driven by a neodymium magnet attached to a DC motor.

Several electrolytes were used for this study, and components were purchased from Sigma-Aldrich, BDH, Mallinckrodt, BDH, and Alpha Aesar and used without further purification. Aqueous acidic iodide electrolytes were prepared in two different concentrations: 0.1 M NaI, 0.1 M H_2SO_4 and 5 mM I_2; and 1 M NaI, 1 M H_2SO_4, and 1 mM I_2. These electrolytes are referred to hereafter as 0.1

M HI and 1 M HI, respectively. Aqueous acid solutions consisting of 0.1 M H_2SO_4 or 1 M H_2SO_4 were also prepared. All water used for the electrolytes and rinsing electrodes was purified to >18 MΩ resistivity using a commercial filtration system (Barnstead). Single-compartment reversible cell measurements used the HI electrolytes, whereas two-compartment HI electrolysis measurements used HI solutions as the positive electrolyte and hydrogen-saturated H_2SO_4 solutions as the negative electrolyte. Potentials were swept at 20 mV sec^{-1}, which allowed for a minimum of hysteresis due to mass-transport in the negative- and positive-going directions.

Current density versus potential (*J*–*E*) data were collected using Princeton Applied Research 273A or VersaStat 3 potentiostats operating in potential-control mode. Unless otherwise noted, the counter electrode was a coiled Pt wire. The reference electrode was Ag/AgCl (3M KCl filling solution, WPI Incorporated) or a homemade Pt pseudo-reference poised at the solution potential. Measurements employing a 2-electrode configuration involved connecting the potentiostat reference lead directly to the coiled Pt wire counter electrode (i.e. shorting the counter and reference electrode leads).

For photoelectrochemistry measurements, illumination was provided by a commercial fiber-optic light source (Thorlabs OSL2) using an EKE type 150-watt halogen bulb (Thorlabs OSL2B). The light intensity was calibrated using a secondary-standard Si photodiode (Thorlabs FDS100-CAL) such that the total flux of photons with greater energy than the Si bandgap (1.1 eV) was equal to that of the AM1.5G reference spectrum. Additional discussion regarding the spectral properties of this light source compared to the solar spectrum is provided in the ESI.

Figures of merit for the n-WSe_2 photoelectrodes were calculated according to the standard conventions for regenerative photoelectrochemistry.[1] Briefly, the open-circuit photovoltage V_{oc} (in volts) was taken as the potential difference between the onset of oxidative photocurrent and the equilibrium potential of the electrolyte of interest (as measured directly by a Pt pseudo-reference). The short-circuit photocurrent density J_{sc} (in mA cm^{-2}) was measured as the current density at the electrolyte equilibrium potential. The dimensionless fill-factor *FF* was taken as the ratio of the maximum power output of the photoelectrochemical cell relative to $V_{oc} \cdot J_{sc}$. Finally, the n-WSe_2|I^- /I_3^- half-cell regenerative solar energy conversion efficiency η_{HC} was calculated on a thermodynamic basis relative to the electrolyte formal potential as

$$\eta_{\mathrm{HC}} = \frac{Voc \cdot Jsc \cdot FF}{P_{\mathrm{in}}} \qquad \text{(Eq. 1)}$$

where P_{in} is the AM1.5G equivalent light intensity (100 mW cm^{-2}). Similarly, the full-cell energy-conversion efficiency for HI-splitting η_{FC} was calculated as

$$\eta_{\mathrm{FC}} = \frac{\Delta E_{\mathrm{FC}} \cdot Jop}{P\mathrm{in}} \qquad \text{(Eq. 2)}$$

where ΔE_{FC} is the full-cell formal potential difference (in volts) between hydrogen evolution and iodide oxidation in the cell as measured at two nonpolarizable electrodes, and J_{op} is the operating current density of the photoelectrode and counter electrode (in mA cm^{-2} and on the basis of the photoelectrode area) when short-circuited to one another. We used two clean Pt electrodes, which are highly reversible for both hydrogen evolution and iodide oxidation, to explicitly measure ΔE_{FC} in this system under conditions identical to those used for photoelectrochemical HI electrolysis.

Impedance data were collected using a Solartron SI 1280B impedance analyzer. Data were collected using a 10 mV, 5 kHz sinusoidal potential waveform superimposed on a DC bias over the range of -0.2 to 0.9 V vs Ag/AgCl. The reference electrode was a Pt wire and the cell was maintained in the dark and in a Faraday cage to minimize extrinsic effects from illumination and electrical noise. Impedance data were fit in the standard fashion for Mott-Schottky analysis using a simple equivalent circuit model over a fixed potential range as described in the ESI.

Results

We collected current-voltage (*J–E*) data for representative n-type WSe_2 photoelectrodes facilitating regenerative (i.e. photovoltaic) iodide oxidation in different electrolyte concentrations and electrode configurations. The *J–E* performance was essentially the same for HI concentrations of 0.1 and 1 M (Figure 3a) and also did not change significantly when transitioning between two-electrode and three-electrode measurements (Figure 3b). Energy-conversion efficiencies for n-WSe_2 photoelectrodes ranged from 2–6% based on a 1-Sun equivalent incident light intensity (100 mW cm^{-2}). Figures of merit for n-WSe_2 photoelectrodes have been compiled in Table 1, and complete data for all of the electrodes included in this study are available in the ESI.

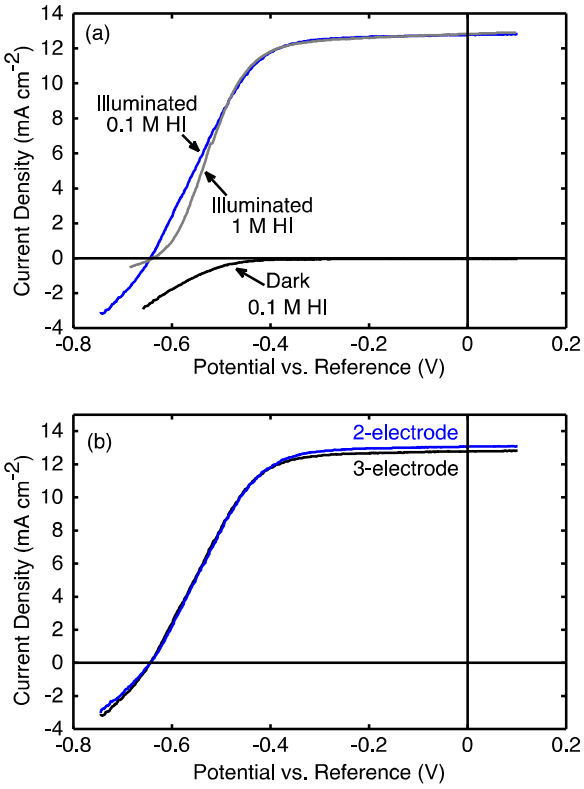

Figure 3. Compiled *J–E* data for a single n-WSe_2 electrode facilitating reversible iodide oxidation while varying (a) the electrolyte concentration and (b) the cell configuration as noted in the panel and described in the Experimental section.

Table 1. Figures of merit for n-WSe_2 regenerative cells[a]

Sample and electrolyte parameters	Voc (V)	Jsc (mA cm^{-2})	*FF*	η_{HC}	N[b]
unetched; 0.1 M HI; 3-electrode	0.63 ± 0.02	13.3 ± 1.4	0.58 ± .05	4.8 ± 0.5	9
unetched; 0.1 M HI; 2-electrode	0.63 ± .01	12.4 ± 1.7	0.59 ± .01	4.7 ± 0.7	3
photo-etched; 0.1 M HI; 3-electrode	0.58 ± 0.04	13.2 ± 4.0	0.53 ± .03	4.1 ± 1.4	7
unetched; 1 M HI; 3-electrode	0.63 ± 0.04	13.2 ± 0.3	0.60 ± .02	5.0 ± 0.4	4

[a]Uncertainty values are taken at 1 standard deviation from the mean.
[b]Number of electrodes tested

We further assessed the stability of n-WSe_2 photoelectrodes facilitating iodide oxidation in aqueous acidic electrolyte. Figure 4a shows the results of a continuous illumination experiment on a representative n-WSe_2 | HI_3/HI half cell in 0.1 M HI electrolyte, which involved holding the cell potential near the maximum power point for 18 hours with cyclic voltammograms collected every

three hours. Over the course of these experiments, the photocurrent clearly decayed to approximately half of its original value, but the photovoltage did not decrease significantly. Upon removal of the photoelectrode from the solution, we observed a reddish-brown crystalline material coating most of the surface, which we took to be solid I_2. After thoroughly rinsing the surface with a mixture of water and ethanol, the *J–E* performance of the n-WSe_2 electrode fully recovered, as shown in Figure 4b. We ran a similar experiment in the 1 M HI electrolyte for >20 hours, during which the photocurrent also diminished somewhat. We found this decrease likely resulted from increasing solution optical absorption as the HI electrolyte was slowly oxidized by air to give more of the highly absorbing aqueous I_3^- anion. Data and discussion for the high-concentration stability experiment are included in the ESI.

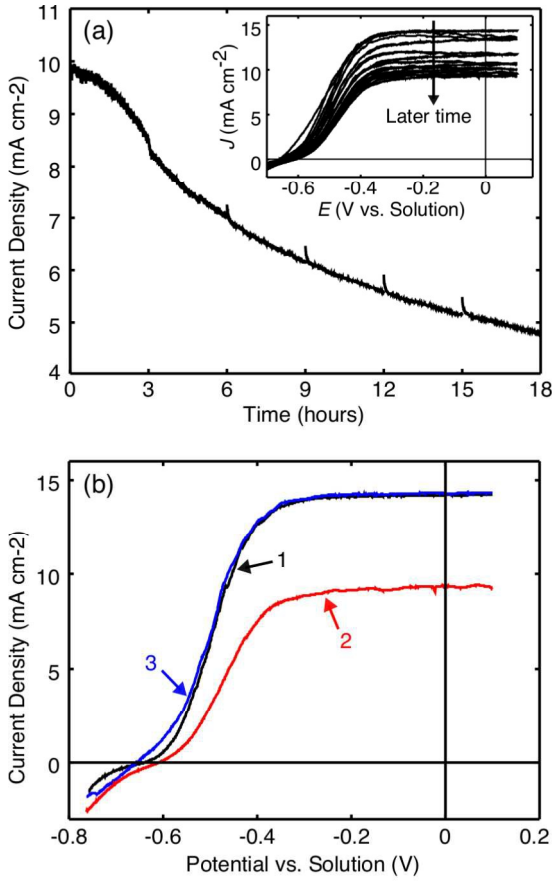

Figure 4. (a) Current versus time data for an illuminated n-WSe_2 photoelectrode held at -0.465 V versus the solution potential for 18 hours. The inset shows corresponding current-potential performance of the electrode at 3-hour intervals. (b) Current-voltage behavior of the same photoelectrode at three different time points: (1) prior to potentiostatic testing, (2) immediately after potentiostatic testing, and (3) after removal of the precipitate that formed during the potentiostatic experiment.

Figure 5 shows the *J–E* behavior of two platinized Pt electrodes carrying out net HI electrolysis from air-saturated 1.0 M HI positive electrolyte and hydrogen-saturated 1.0 M H_2SO_4 negative electrolyte, using a two-compartment acrylic cell with a Nafion separator. The open-circuit potential of this cell was 0.42 V, which was used as the value of ΔE_{FC} for the purposes of calculating full-cell energy conversion efficiencies (Eq. 2). Overlaid against these Pt-Pt data, are the solar conversion data for two representative n-WSe_2 electrodes. As has been shown previously, the intersection point between these datasets can serve as a prediction for the operating current density for the energy-storage cell operating with an illuminated semiconductor short-circuited to a counter electrode.[13,51,52] This approach yielded an average predicted operating current density of 9.7 ± 1.6 mA cm^{-2} (n=4).

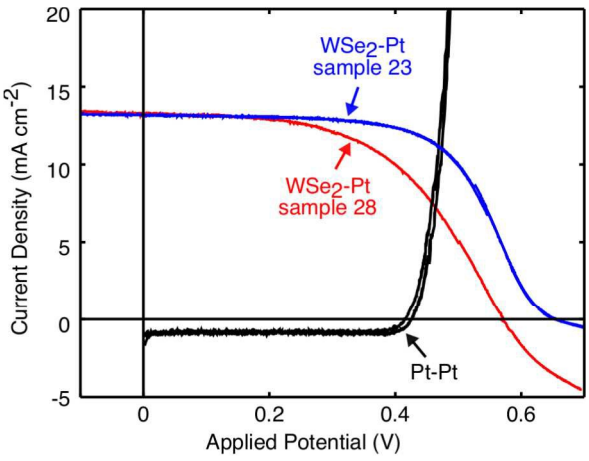

Figure 5. *J–E* data for two n-WSe_2 photoelectrodes facilitating reversible iodide oxidation in a 3-electrode configuration overlaid against corresponding data for HI electrolysis at two Pt electrodes. The WSe_2 data were collected under simulated AM1.5 illumination in 1.0 M HI electrolyte, and the potential axis was inverted relative to the standard convention so as to treat the photoelectrochemical cell as an energy input for the HI electrolysis reaction. The Pt-Pt HI electrolysis data were collected in the two-compartment cell with air-saturated 1.0 M HI positive electrolyte and hydrogen-saturated 1.0 M H_2SO_4 negative electrolyte.

Cyclic voltammetry data for HI electrolysis from the same two n-WSe_2 photoelectrodes contacted to a ~0.13 cm^2 platinized Pt counter in a separate compartment are shown in Figure 6a. Figure 6b also shows current versus time data for these electrodes illuminated under short-circuit conditions. The light was manually chopped at 0.1 Hz to confirm that the observed current was photo-induced. The actual average operating current density (with respect to the semiconductor area) at short-circuit was 10.0 ± 1.6 mA cm^{-2} (n=4), which corresponds to $\eta_{FC} = 4.2 \pm 0.7$ %.

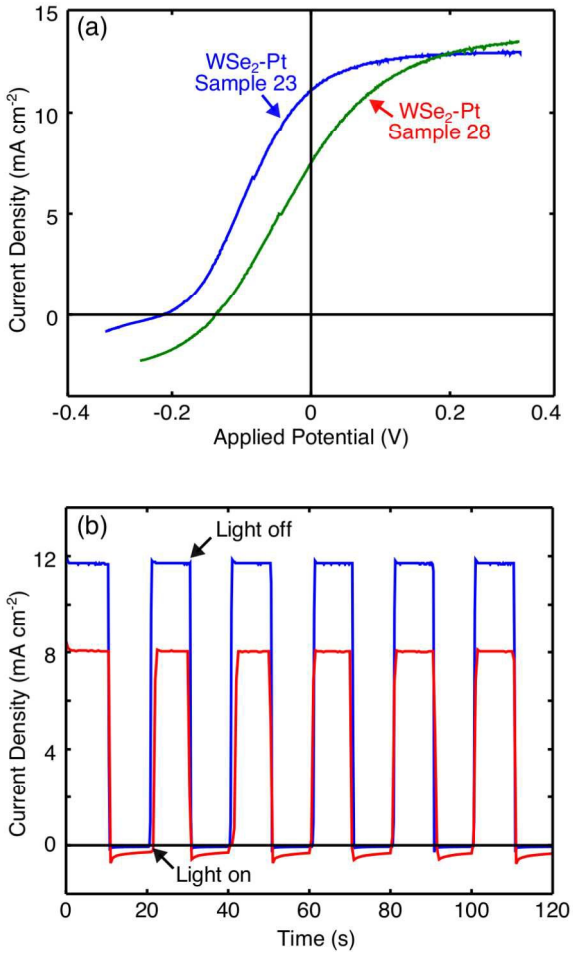

Figure 6. (a) *J–E* behavior of two illuminated n-WSe_2 electrodes in 1.0 M HI electrolyte measured in a two-electrode configuration against a Pt counter electrode in a separate compartment filled with hydrogen-saturated 1.0 M H_2SO_4 electrolyte. (b) Potentiostatic measurements of the same two electrodes illuminated under short-circuit conditions in the same respective electrolytes. The light was manually chopped at 0.1 Hz.

To elucidate the energetics of the n-WSe_2|HI_3/HI interface, we carried out electrochemical impedance spectroscopy and Mott-Schottky (M–S) analysis.[53] Representative M–S data are shown in Figure 7a, and compiled data for flatband potentials, as a function of iodide concentration, are shown in Figure 7b. For convenience, the vertical axis of 7a is plotted as an "M–S Factor" in units of $cm^3 \cdot V$ such that the inverse of the slope is equal to the doping density. Complete discussion of the M–S methodology is provided in the ESI. The data were generally linear over a range of several hundred mV, and flatband potentials were highly sensitive to the solution iodide concentration, shifting by >600 in the negative direction between 0 and 1.0 M iodide.

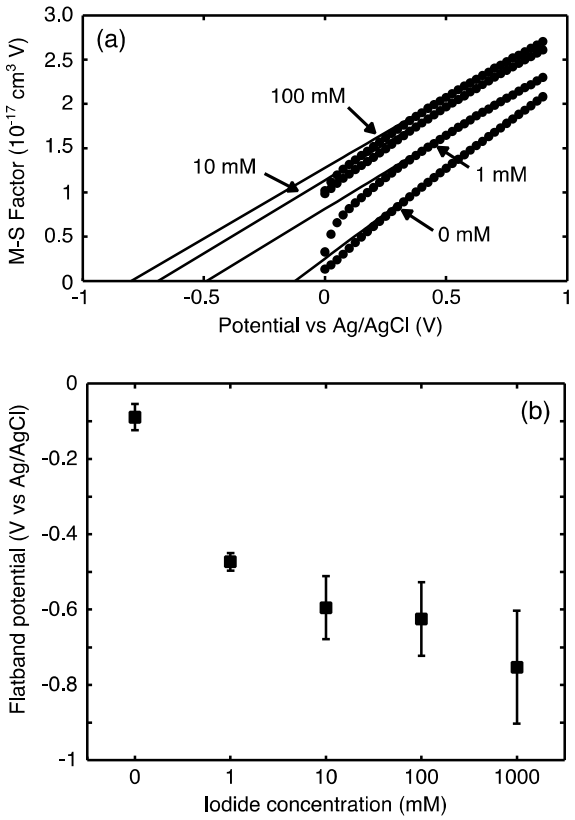

Figure 7. (a) Representative Mott-Schottky data for n-WSe_2 photoelectrodes collected in aqueous 0.1 M H_2SO_4 electrolyte with the addition of the noted concentrations of NaI. (b) Compiled flatband potentials for n-WSe_2 electrodes as a function of iodide concentration. In all cases the electrolyte contained the noted concentration of NaI and 0.1 M H_2SO_4, except in the case of 1.0 M iodide, which contained 1.0 M H_2SO_4. The error bars represent one standard deviation in the measured values from three different electrodes.

Discussion

Very high photoelectrochemical energy conversion efficiencies have been reported previously for n-WSe_2 photoelectrodes under laboratory illumination,[39,40,54] although reported efficiencies in outdoor sunlight were somewhat lower.[41] Our results broadly agree with these experiments, attesting to the viability of this material, and the layered metal dichalcogenides in general, as attractive candidates for robust electrochemical solar energy conversion. The high absorption coefficient of triiodide electrolytes below 500 nm, however, significantly limits the obtainable photocurrent densities for WSe_2 photoelectrodes in full sunlight due to parasitic absorption in the electrolyte itself. These losses might be mitigated by limiting the optical path length through which the light must transmit.

Very high stabilities have been reported previously for n-$MoSe_2$ | I_3^-/I^- cells.[41,42] Our results suggest

that n-WSe_2 is also highly stable, even in strongly acidic iodide electrolyte. However, we observed a sizeable decrease in photocurrent density for n-WSe_2 electrode during light-soaking measurements. We attribute the decrease to precipitation of solid I_2 crystals on the surface of the electrode during measurements in 0.1 M HI electrolyte, leading to diminished light absorption and physical blocking of the electrode surface from contact with the electrolyte. This effect has been observed previously for n-WSe_2 electrodes subjected to high light intensities in more concentrated iodide electrolytes. It is plausible that the rate of I_2(s) solvation by I^-(aq) to generate the I_3^-(aq) anion is sufficiently slow that the surface oxidation reaction "outruns" the solvation, leading to I_2(s) precipitation. The effect could be suppressed by increasing the HI concentration, which should increase the rate of I_2 dissolution. However, we found that concentrated HI solutions were prone to spontaneous oxidation in air, resulting in darkening of the electrolyte and somewhat diminished photocurrents. Further experiments are warranted to fully elucidate WSe_2 phtoelectrode stability and the competition between oxidation and dissolution at or near the WSe_2 surface as a function of light intensity and electrolyte concentration.

Our results agree with those of Bicelli and Razzini, who previously reported unassisted HI splitting on n-WSe_2.[45] However, that study involved intense visible illumination by a focused light source in a microscope, which only permitted observation of HI-splitting qualitatively by simultaneous observation of bubbles and dark red crystals. Our experimental configuration allowed independent electrochemical characterization of the WSe_2 photoelectrodes and the HI electrolyte as well as explicit coulometric measurements of the HI electrolysis rate, which together facilitate a much clearer picture of the overall energy storage process.

Our n-WSe_2 photoelectrodes gave aqueous HI electrolysis at $J > 10$ mA cm^{-2}, which corresponds to > 4 % energy storage efficiency. This value is comparable to that reported for solar water splitting using multi-junction amorphous Si solar cells,[14] but it is substantially lower than several values recently reported using high-quality photovoltaic devices.[15,16] The simplicity of our approach is attractive, however, in that it requires only one semiconductor electrode with an ohmic back contact, a counter electrode, and a suitable cell housing that incorporates a proton-exchange membrane. Thus many of the processing steps involved in generating semiconductor homojunctions and fabricating a functional photovoltaic are obviated in this case. Improving the WSe_2 crystal quality and optimizing the cell design to improve photocurrent would likely lead to

significantly greater device efficiencies. Surface texturing could also be used to lower reflection losses at the semiconductor surface, although texturing methods would also need to preserve or improve the quality of the rectifying junction.

Our Mott–Schottky results are broadly in agreement with previous measurements of the iodide concentration dependence of the band edge positions for n-WSe_2.[55] The negative shift in the flatband potential is consistent with specific adsorption of negatively charged I^-(aq) and/or I_3^-(aq) on the semiconductor surface. The shift results in a large increase in the interfacial barrier height, giving rise to large photovoltages. Indeed, Lewis calculated that the maximum obtainable V_{oc} value for WSe_2 semiconductors in the bulk-recombination limit is on the order of 0.7 V.[56] This value is only ~50 mV larger than the largest values we observed from electrolytes containing $[I^-] \geq 0.1$ M.

In addition to providing for large photovoltages in regenerative iodide oxidation, the band edge shift due to iodide adsorption is critically important in allowing n-WSe_2 to facilitate net HI electrolysis without an external bias. Figure 8 schematizes the relationship between the n-WSe_2 band edges and the H^+/H_2 and I_3^-/I^- redox couples. In the absence of iodide, the conduction band edge is not sufficiently negative to drive hydrogen evolution at a counter electrode at an appreciable rate (Fig. 8a). Upon adsorption of iodide, the bands shift significantly in the negative direction (Fig. 8b), which facilitates significant band bending upon equilibration (Fig. 8c) and nearly optimal band edge positions for HI electrolysis when illuminated and short-circuited to a Pt counter electrode (Fig. 8d). This outcome serves to illustrate the importance of surface chemistry in dictating the interfacial energetics of photoelectrochemical cells, particularly those involving semiconductor-liquid junctions.

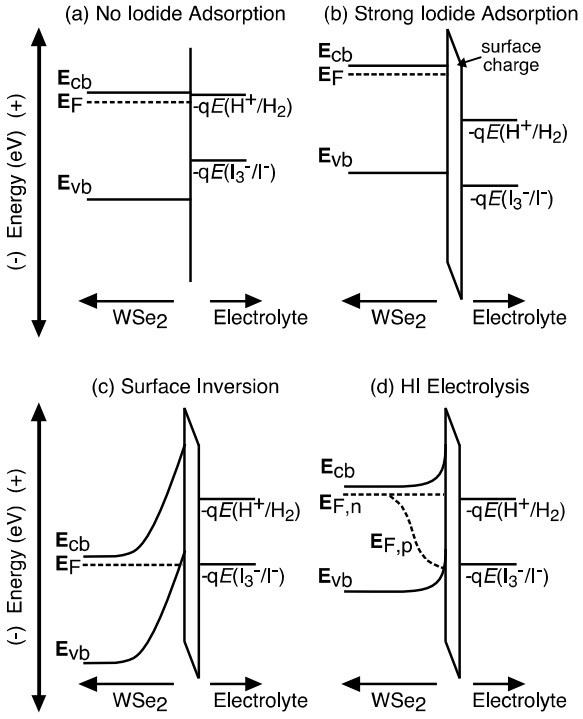

Figure 8. Band energy versus position diagrams for the n-WSe_2–HI(aq) interface: (a) hypothetical interfacial relationships before equilibration in the absence of surface adsorption; (b) actual interfacial relationships before equilibration, accounting for iodide surface adsorption; (c) band energetics after equilibration in the dark, resulting in strong band-bending and a surface inversion layer; (d) band energetics during unassisted HI photoelectrolysis showing sufficient quasi-Fermi level splitting to drive hydrogen evolution and iodide oxidation at an appreciable rate.

Conclusions

We have demonstrated that crystalline n-type WSe_2 photoelectrodes are capable of facilitating unassisted HI electrolysis from acidic iodide electrolytes when paired with a suitable counter electrode. These photoelectrodes also show high regenerative energy-conversion efficiencies and good stabilities, in accordance with previous observations. The ability of n-WSe_2 to split HI stems from specific surface interactions with iodide, which shift the band edges significantly negative on the electrochemical scale. The high resulting efficiencies and stabilities exhibited by n-WSe_2 photoelectrodes make this material, and related layered dichalcogenides, promising for further study in the context of solar-driven galvanic energy storage.

References

(1) Tan, M. X.; Laibinis, P. E.; Nguyen, S. T.; Kesselman, J. M.; Stanton, C. E.; Lewis, N. S. In *Progress in Inorganic Chemistry*; Karlin, K. D., Ed.; Wiley, 1994; Vol. 41, pp 21–144.

(2) Nozik, A. *Annu. Rev. Phys. Chem.* **1978**, *29*, 189.

(3) Nozik, A. J.; Memming, R. *J. Phys. Chem.* **1996**, *3654*, 13061.

(4) McDowell, M. T.; Lichterman, M. F.; Spurgeon, J. M.; Hu, S.; Sharp, I. D.; Brunschwig, B. S.; Lewis, N. S. *J. Phys. Chem. C* **2014**, *118*, 19618.

(5) Hu, S.; Shaner, M. R.; Beardslee, J. A.; Lichterman, M.; Brunschwig, B. S.; Lewis, N. S. *Science* **2014**, *344*, 1005.

(6) Chen, Y. W.; Prange, J. D.; Dühnen, S.; Park, Y.; Gunji, M.; Chidsey, C. E. D.; McIntyre, P. C. *Nat. Mater.* **2011**, *10*, 539.

(7) Kenney, M. J.; Gong, M.; Li, Y.; Wu, J. Z.; Feng, J.; Lanza, M.; Dai, H. *Science* **2013**, *342*, 836.

(8) Yang, J.; Walczak, K.; Anzenberg, E.; Toma, F. M.; Yuan, G.; Schwartzberg, A.; Lin, Y.; Hettick, M.; Javey, A.; Ager, J. W.; Yano, J.; Frei, H.; Sharp, I. D. *J. Am. Chem. Soc.* **2014**, *136*, 6191.

(9) Strandwitz, N. C.; Comstock, D. J.; Grimm, R. L.; Nichols-Nielander, A. C.; Elam, J.; Lewis, N. S. *J. Phys. Chem. C* **2013**, *117*, 4931.

(10) Seger, B.; Pedersen, T.; Laursen, A. B.; Vesborg, P. C. K.; Hansen, O.; Chorkendor, I. *J. Am. Chem. Soc.* **2013**, *135*, 1057.

(11) Scheuermann, A. G.; Prange, J. D.; Gunji, M.; Chidsey, C. E. D.; McIntyre, P. C. *Energy Environ. Sci.* **2013**, *6*, 2487.

(12) Paracchino, A.; Laporte, V.; Sivula, K.; Grätzel, M.; Thimsen, E. *Nat. Mater.* **2011**, *10*, 456.

(13) Walter, M. G.; Warren, E. L.; McKone, J. R.; Boettcher, S. W.; Mi, Q.; Santori, E. a.; Lewis, N. S. *Chem. Rev.* **2010**, *110*, 6446.

(14) Reece, S. Y.; Hamel, J. A.; Sung, K.; Jarvi, T. D.; Esswein, A. J.; Pijpers, J. J. H.; Nocera, D. G. *Science* **2011**, *334*, 645.

(15) Cox, C. R.; Lee, J. Z.; Nocera, D. G.; Buonassisi, T. *Proc. Natl. Acad. Sci.* **2014**, *111*, 14057.

(16) Luo, J.; Im, J.-H.; Mayer, M. T.; Schreier, M.; Nazeeruddin, M. K.; Park, N.-G.; Tilley, S. D.; Fan, H. J.; Gratzel, M. *Science* **2014**, *345*, 1593.

(17) Khaselev, O.; Turner, J. A. *Science* **1998**, *280*, 425.

(18) Licht, S.; Wang, B.; Mukerji, S.; Soga, T.; Umeno, M.; Tributsch, H. *J. Phys. Chem. B* **2000**, *104*, 8920.

(19) Khaselev, O.; Bansal, a.; Turner, J. a. *Int. J. Hydrogen Energy* **2001**, *26*, 127.

(20) Kainthla, R. C.; Zelenay, B.; Bockris, J. O. *J. Electrochem. Soc.* **1985**, *134*, 841.

(21) Bolton, J. R.; Strickler, S. J.; Connolly, J. S. *Nature* **1985**, *316*, 495.

(22) Braff, W. a; Bazant, M. Z.; Buie, C. R. *Nat. Commun.* **2013**, *4*, 2346.

(23) Livshits, V.; Ulus, a.; Peled, E. *Electrochem. commun.* **2006**, *8*, 1358.

(24) Huskinson, B.; Rugolo, J.; Mondal, S. K.; Aziz, M. J. *Energy Environ. Sci.* **2012**, *5*, 8690.

(25) Singh, N.; Mubeen, S.; Lee, J.; Metiu, H.; Moskovits, M.; McFarland, E. W. *Energy Environ. Sci.* **2014**, *7*, 978.

(26) Khaselev, O.; Turner, J. A. *Electrochem. Solid-State Lett.* **1999**, *2*, 310.

(27) Nakato, Y.; Jia, J. G.; Ishida, M.; Morisawa, K.; Fujitani, M.; Hinogami, R.; Yae, S. *Electrochem. Solid-State Lett.* **1998**, *1*, 71.

(28) Nakato, Y.; Egi, Y.; Hiramoto, M.; Tsubomura, H. *J. Phys. Chem.* **1984**, *88*, 4218.

(29) Johnson, E. *IEEE Electron Devices Meet. 1981* **1981**, *27*, 2.

(30) Mubeen, S.; Lee, J.; Singh, N.; Moskovits, M.; McFarland, E. W. *Energy Environ. Sci.* **2013**, *6*, 1633.

(31) Ardo, S.; Park, S. H.; Warren, E. L.; Lewis, N. S. *Energy Environ. Sci.* **2015**, DOI: 10.1039/C5EE00227C.

(32) *Photoelectrochemistry and Photovoltaics of Layered Semiconductors*; Aruchamy, A., Ed.; Physics and Chemistry of Materials with Low-Dimensional Structures; Kluwer: Norwell, MA, 1992; Vol. 14.

(33) Bouroushian, M. *Electrochemistry of Metal Chalcogenides*; 2010; pp 57–76.

(34) Fan, F. F.; White, H. S.; Wheeler, B.; Bard, A. J. *J. Electrochem. Soc.* **1980**, *127*, 518.

(35) Kautek, W.; Gerischer, H. *Electrochim. Acta* **1981**, *26*, 1771.

(36) Bicelli, L. P.; Razzini, G. *Surf. Technol.* **1982**, *16*, 37.

(37) Razzini, G.; Lazzari, M.; Bicelli, L. P.; Levy, F.; De Angelis, L.; Galluzzi, F.; Scafé, E.; Fornarini, L.; Scrosati, B. *J. Power Sources* **1981**, *6*, 371.

(38) Fan, F.-R. F.; Bard, A. J. *J. Electrochem. Soc.* **1979**, *128*, 945.

(39) Tenne, R.; Wold, A. *Appl. Phys. Lett.* **1985**, *47*, 707.

(40) Prasad, G.; Srivastava, O. N. *J. Phys. D. Appl. Phys.* **1988**, *21*, 1028.

(41) Kline, G.; Kam, K.; Canfield, D.; Parkinson, B. a. *Sol. Energy Mater.* **1981**, *4*, 301.

(42) Tributsch, H. *Sol. Energy Mater.* **1979**, *1*, 257.

(43) Fan, F.-R. F.; White, H. S.; Wheeler, B. L.; Bard, A. J. *J. Am. Chem. Soc.* **1980**, *102*, 5142.

(44) Levy-Clement, C.; Heller, A.; Bonner, W.; Parkinson, B. *J. Electrochem. Soc.* **1981**, *129*, 1701.

(45) Bicelli, L. P.; Razzini, G. *Surf. Technol.* **1983**, *20*, 393.

(46) Baglio, J. A.; Calabrese, G. S.; Kershaw, R.; Kubiak, C. P.; Riccot, A. J.; Wold, A.; Wrighton, M. S.; Zoski, G. D. *J. Electrochem. Soc.* **1982**, *129*, 1461.

(47) Srivastava, S. K.; Avasthi, B. N. *J. Mater. Sci.* **1985**, *20*, 3801.

(48) Koval, C.; Olson, J. *J. Electroanal. Chem.* **1987**, *234*, 133.

(49) Legma, J. B.; Vacquier, G.; Casalot, a. *J. Cryst. Growth* **1993**, *130*, 253.

(50) Mahalu, D.; Jakubowicz, A.; Wold, A.; Tenne, R. *Phys. Rev. B* **1988**, *38*, 1533.

(51) Weber, M. F.; Dignam, M. J. *J. Electrochem. Soc.* **1984**, *131*, 1258.

(52) Winkler, M.; Cox, C.; Nocera, D.; Buonassisi, T. *Proc. Natl. Acad. Sci.* **2013**, *110*, E1076.

(53) Orazem, M. E.; Tribollet, B. *Electrochemical Impedance Spectroscopy*; The Electrochemical Society Series; Wiley: Hoboken, NJ, 2008.

(54) Campet, G.; Azaiez, C.; Levy, F.; Bourezc, H.; Claverie, J. *Act. Passiv. Electron. Components* **1988**, *13*, 33.

(55) Lewerenz, H. J.; Gerischer, H.; Lübke, M. *J. Electrochem. Soc.* **1984**, *131*, 100.

(56) Lewis, N. S. *J. Electrochem. Soc.* **1984**, *131*, 2496.

Figures and Tables

For convenience, Figures and tables have been provided inline in the manuscript text.

Acknowledgements

This work was supported by the Energy Materials Center at Cornell, an Energy Frontier Research Center funded by the US Department of Energy, Office of Basic Energy Sciences under Award Number DE-SC0001086. JRM additionally acknowledges the U.S. Department of Energy, Office

of Energy Efficiency and Renewable Energy for a SunShot postdoctoral research award. RAP acknowledges the National Science Foundation for research support through the Integrative Graduate Education and Research Traineeship (IGERT) program.

Supporting Information Available

The following additional data and discussion are available in the Electronic Supporting Information: schematics and photographs of electrochemical cells; comparison of halogen light source to the AM1.5G spectrum; discussion of light absorption by triiodide electrolytes; complete photoelectrode figures of merit; stability data for an n-WSe_2 photoelectrode in contact with 1M HI electrolyte; details of Mott–Schottky methodology and reproducibility.

Table of Contents Graphic and Summary

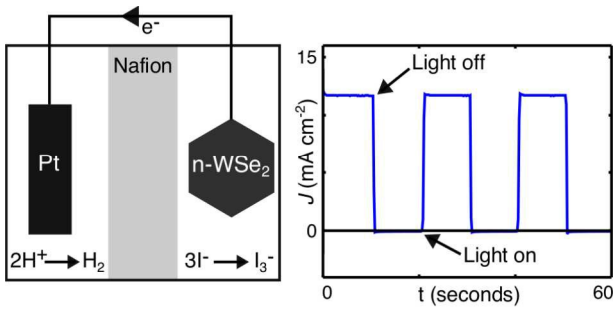

A single n-WSe_2 photoelectrode, electrically connected to a Pt counter electrode, can drive unassisted HI electrolysis under solar-simulated illumination.